Published in final edited form as:

Chembiochem. 2019 February 15; 20(4): 526–531. doi:10.1002/cbic.201800495.

Cell-compatible Nanoprobes for Imaging Intracellular Phosphatase Activities

Jiaqing Wang[a], **Jie Zhou**[a], **Hongjian He**[a], **Difei Wu**[a], **Xuewen Du**[a], and **Dr. Bing Xu**[a] **[Prof]**

[a]Department of Chemistry, Brandeis University, 415 South St. Waltham, MA 02454 (USA), bxu@brandeis.edu

Abstract

Phosphatases play an important role in cell biology, but there are few suitable probes for selectively imaging phosphatase activity of live cells because the current probes require cell fixation or exhibit considerable cytotoxicity. Here we show that conjugating a D-peptide to a quinazolinone derivative generates cell-compatible, biostable probes for imaging phosphatase activities inside live cells. Moreover, our results show that inhibiting ectophosphatases is a critical factor for imaging intracellular phosphatases. As the first example of using selective inhibitors to ensure intracellular function of molecular probes, this work illustrates a facile approach to design molecular probes for profiling the activities of enzymes in spatial selective manner in a complicated environment.

Graphical Abstract

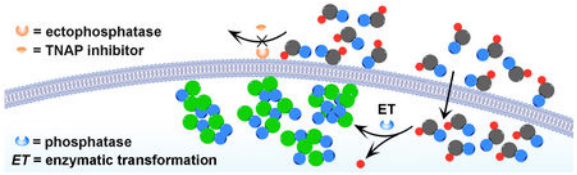

This work reports a conjugate of D-peptide and quinazolinone as cell-compatible, biostable imaging probes for imaging phosphatase activities inside live cells, which illustrates a facile approach to design molecular probes for profiling the activities of enzymes in spatial selective manners.

Keywords

Intracellular phosphatase; ectophosphatase; selectivity; live cells; molecular probe

---

Being controlled by kinase/phosphatase enzyme switch, protein phosphorylation/dephosphorylation is the most common post-translational mechanism for modulating the functions of proteins in a wide range of cellular processes.[1] Thus, phosphatases play key regulatory roles in many physiological processes, including immune response,[2] pathogen virulence,[3] cancer cell proliferation and metastasis,[4] and host-microbe interaction.[5] More specifically, phosphatases, which catalyze the hydrolysis of phosphorylated substrates,

are necessary for embryogenesis,[6] bone formation,[7] and neuron signaling.[8] In addition, certain phosphatases have associated with cancers[4] and have served as tumor markers[4a] for a number of cancers (e.g., pancreatic, ovarian, and testis).[9]

Despite the importance of phosphatases,[1, 10] the activity probes[11] of phosphatase remain less developed.[12] Although there are several agents for detecting phosphatases, they still suffer serious shortcomings. The conventional color assay (p-nitrophenyl phosphate (PNPP) [13]), though being able to detect the presence of phosphatases, is unsuitable for live cell imaging due to the lack of sensitivity. The fluorescent staining agent (ELF®97), which bases on restricting bond rotation to generate fluorescent colloids,[14] still requires cell fixation during the histological sample preparation,[15] and is unsuitable for activity profiling of phosphatases in live cells. The quinazolinone analogs of ELF®97 are unable to achieve satisfactory results on live cells due to its irreversible nucleated crystallization,[16] significant cytotoxicity, or poor spatial resolution.[17] The recently reported D-peptide based phosphatase probes are more suitable to imaging ectophosphatases[18] than intracellular phosphatases of live cells. But many phosphatases associated cellular processes occur intracellularly such as phosphoprotein phosphatase (PPP) family of Ser/Thr protein phosphatases and intracellular pTyr-specific phosphatases (PTPs) including PTP1B, SHP2, and MEG2.[19] Therefore, there still are unmet needs to develop functional probes for imaging the activities of intracellular phosphatases of live cells with high spatiotemporal resolution. To address this previously overlooked problem, we decide to develop a new approach for generating molecular probes that are selective for imaging intracellular phosphatases.

Here we show that the combination of a quinazolinone and a D-tripeptide results a new type of imaging probes that are cell compatible and bio-stable, preserve the sensitivity and excellent imaging contrast of ELF®97, and eliminate the uncontrolled formation of microcrystals without compromising the non-diffusiveness of the probes. Our results show that these probes, working at a wide concentration range, are capable of imaging phosphatase activities inside live cells when ectophosphatases are inhibited (Scheme 1). Illustrating a simple strategy that incorporates D-peptides to generate non-diffusive, amorphous, and biocompatible imaging probes for revealing the activities of intracellular enzymes in complicated cellular environment in the presence of a proper inhibitor, this work contributes to the development of activity probes of important enzymes.

Scheme 1 shows the design of the D-peptide conjugated molecular probes containing a quinazolinone derivative that is based on ELF®97. As a good substrate for phosphatases, ELF®97 has several unique merits, including significant signal changes, excellent photo stability, and prompt responses. Upon enzymatic cleavage, ELF®97, from being soluble and weakly blue-fluorescent, yields a bright green fluorescent precipitate.[14] However, the use of ELF®97 requires the fixation of cells and is unsuitable for live cells. Moreover, the dephosphorylation of ELF®97 results in uncontrolled crystallization that is detrimental for achieving high spatial resolution within a single cell. To achieve live cell imaging, to target exclusively intracellular phosphatases, and to eliminate uncontrolled nucleation of the crystallization, we modify ELF®97 with a small D-peptide sequence (^{D}Phe-^{D}Phe-^{D}Tyr) to yield precursor **1**. In addition, we choose to use neutral small functional group for replacing

the carboxylic acid group at the C-terminus of the peptides for enhancing their self-assembling ability.[20] Such a design not only preserves the excellent fluorescence of ELF®97, but also efficiently changes the crystallization to a self-assembly process since the sequence of ^{D}Phe-^{D}Phe-^{D}Tyr have been proven to be an excellent motif for self-assembly.[20–21]

Scheme S1 shows the synthetic route based on the design. We use a multi-step synthesis to generate the phosphorylated quinazolinone derivative (**3**), then use solid phase peptide synthesis (SPPS)[22] to obtain intermediates (**4**) that contain carboxylic acid group at C-terminus, and finally select methylacetate (-COOMe) or *N*-methylacetamide (-CONHMe) group to replace the carboxylic acid terminus of **4** to result in D-peptide conjugated quinazolinone derivatives, **1a** or **1b**, respectively. The difference of **1a** and **1b** is that **1a** is a substrate of carboxylesterases, but **1b** is not.

As shown in the insets of Figure 1a, **1a** (or **1b**) forms a transparent solution. Transmission electron microscopy (TEM) images show that the solution of **1a** contains sparse nanofibers (8 nm ± 2 nm) while the solution of **1b** produces aggregates (with the particle sizes of 8–19 nm) upon drying. After the addition of alkaline phosphatase (ALP), the solution of **1a** becomes a stable hydrogel, which exhibits bright green fluorescence under UV irradiation, and the solution of **1b** transforms to a viscous liquid that shows yellow fluorescence. As revealed by TEM, the hydrogel contains dense nanofibers (diameter of ~8 nm), and the viscous liquid consists of the mixture of nanofibers (diameter of ~8 nm) and aggregates (particle sizes of 8–19 nm). Before the addition of ALP, static light scattering (SLS) (Figure 1b) of the solutions of **1a** and **1b** exhibits signals slightly higher than and almost the same as that of PBS buffer, respectively. The intensities of the SLS signals increase drastically after the addition of ALP to the solutions. These results confirm that soluble precursors **1a** and **1b** become fluorescent and insoluble nanofibers or aggregates after the dephosphorylation catalyzed by the phosphatases. The precursor **1a** undergoes ALP catalyzed dephosphorylation, but only reaches 50% conversion after 30 h when the concentration of ALP is 0.1 U/mL (Figure 1c and S1). The incomplete dephosphorylation likely is resulted from the incorporation of the precursors into the nanofibers. So the nanofibers consist of **1a** and **2a**. The precursor **1b** also dephosphorylated with the addition of ALP but only achieves 31% conversion after 30 h (Figure S2), corresponding with the TEM that exhibits a mixture of nanofibers and aggregates.

After confirming that dephosphorylation of **1a** results in a fluorescent gel of **2a**, we incubate Saos-2 cells with **1a** and monitor the change of the fluorescence in the cell culture. We choose Saos-2 cells because they, overexpressing tissue non-specific alkaline phosphatase (TNAP,[23] an ectophosphatase), offer a fine case to test the probes in a complicated environment (i.e., extracellular and intracellular phosphatases co-existing). The time-dependent fluorescence of **2a** (Videos S1 and S2 in SI) reveals the extracellular and intracellular distribution of phosphatases without and with a TNAP inhibitor (2,5-dimethoxy-N-(quinolin-3-yl) benzenesulfon-amide (DQB)[24]). As shown in the fluorescent images of live Saos-2 cells at different time points (0 min, 15 min, and 30 min (Figure 1d)), the fluorescence of **2a** appears in the cytoplasm, suggesting that the cells uptake **1a** and the intracellular phosphatases turn **1a** to **2a** to result in the fluorescence. Without the addition of

any phosphatase inhibitor, beside the bright fluorescence in the cytoplasm, considerable amount of fluorescent spots exist outside cells. While the intracellular fluorescence increases moderately from 15 to 30 min, the amount of extracellular fluorescent particles increases considerably. This result, besides agreeing with that dephosphorylating **1a** generates insoluble, fluorescent **2a**, indicates that ectophosphatases (e.g., TNAP) or the phosphatases in the culture medium exhibit different dynamics from intracellular phosphatases. Considering that TNAP is overexpressed on Saos-2 cells, we treat the cells with DQB, the TNAP inhibitor, 2 h before imaging, then co-culture the cells with **1a** and DQB together during imaging. As shown in Figure 1d, after the addition of DQB, extracellular fluorescence reduces significantly, indicating that inhibiting ectophosphatases reduces the dephosphorylation of **1a** outside cells effectively. On the other hand, the intracellular fluorescent increases over time, indicating that the inhibition of ectophosphatases improves the accuracy of imaging the activity of intracellular phosphatase. Although the fibers and aggregates in TEM images of dried samples indicate that the probes might self-assemble before activation, the probe, in fact, dissolves well in water and culture medium at the concentration used. From both of time-dependent and dephosphorylation process of **1a** with the addition of ALP (Figure 1c) and the time-dependent fluorescence of **1a** in live Saos-2 cells within 30 min (Figure 1d), one can conclude that the activation of the probe is fast. In addition, the fluorescence appears after dephosphorylation rather self-assembly. Because the aggregation rate is relevant to phosphatase imaging in live cells, it is important to choose the concentrations of the probes according to cell types or treat the cells with the probes of a series of concentrations for rate determination.

In order to investigate the intracellular uptake of the imaging probe more accurately, we select HeLa cells as the model cells to avoid the influence of too much extracellular fluorescence since it is known that expression of ectophosphatases on HeLa cells is less than on Saos-2 cells.[18b] We incubate HeLa cells with **1a** at different concentration (i.e., 5, 10, 50, and 100 μM) for 4 h, and then switch to fresh live cell imaging solution. When the incubating concentration is 5 or 10 μM, we can hardly observe any fluorescence, suggesting the cellular uptake is less pronounced at such low concentration (Figure S3). It appears that 50 μM of **1a** is sufficient to reveal the distribution of intracellular phosphatase because the fluorescence increases only slightly with **1a** at 100 μM (Figure 1e). We also measured the photostability of **1a** by irradiating the cells for 10 minutes and found that the fluorescence of the probe hardly reduced. This observation (Figure S9) indicates the excellent photostability of the assemblies of the probes. In the optimal condition, we next use confocal microscopy to examine the intracellular localization of **2a** in HeLa cells. As shown in Figure 1f, most of the green fluorescence in the HeLa cells co-localize well with the fluorescence from endoplasmic reticulum (ER) tracker, suggesting that intracellular phosphatases such as PTP1B likely dephosphorylate **1a** to form **2a**. This result agrees with our previous report.[25] As PTP1B is a phosphatase known to localize at the cytoplasmic face of the ER, we used an inhibitor of PTP1B (CinnGEL) to co-incubate with the HeLa cells and **1a** (Figure S10). Increasing the concentration of CinnGEL results in weak fluorescence, confirming that PTP1B is likely the major phosphatase for catalyzing the dephosphorylation of **1a** and activating the probes.

We also apply **1a** on other human cell lines, including four cancer cell lines (HepG2, MCF7, VCaP, and PC-3 cells) and one normal cell line (HS-5), to compare the activities of intracellular phosphatases (Figure 1g and S4). After 4 h of incubation with **1a**, HepG2, MCF7, or PC-3 cells only exhibit weak fluorescence, suggesting the lower activity of their intracellular phosphatases than those of intracellular phosphatases of HeLa cells. Compared with these cells lines, VCaP cells exhibit a little brighter fluorescence but still much weaker than that on Saos-2 and HeLa cells. As a normal cell line, HS-5 cell hardly exhibits fluorescence, indicating low activity of phosphatases inside the cells, consistent with the results using commercially available ELF®97 (Figure S6). This result agrees with dysregulation of phosphorylation and dephosphorylation in malignant cells.[26] To further examine the distribution of the probes when they are incubated with Saos-2 and HeLa cells, we use confocal microscopy to generate 3D constructions of the fluorescence. Figure 1h shows that most of fluorescent puncta distribute through the cytoplasms, with a small amount of extracellular fluorescence remains. This result further proves **1a** is sensitive for imaging phosphatases and selective to reveal the activities intracellular phosphatases. Our study also shows that the probes exhibit slightly toxicity to HeLa and Saos-2 cells, but are largely innocuous to HepG2 and HS-5 cells (Figure S11). This result suggests that overexpressed ALP on HeLa and Saos-2 cells, indeed, is responsible for the conversion of **1a** to **2a** and the subsequent inhibition of these two types of cancer cells.

Considering that the culture media contain soluble esterases,[27] we incubate HeLa, Saos-2, HepG2, or HS-5 cells with the molecular probe **1b**, to avoid the interference of esterase. Being treated by **1b**, HeLa or Saos-2 cells exhibit bright fluorescence, which is comparable to the fluorescence from the same cells treated **1a**. There is hardly any fluorescence in HepG2 and HS-5 cells after being treated by **1b** (Figure 2a). This result suggests negligible amount of esterases in culture media has minimal impact on **1a**. However, the addition of exogenous carboxylesterase (CES) (e.g., 1 U/mL) significantly decreased the fluorescence when we incubate Saos-2 cells with the probe **1a**, and the fluorescence become weaker gradually with the amount of CES increasing (Figure S5). These observations further support our design that using small neutral group to capping the C-terminals of the peptides enhances their self-assembling ability.

We carry out a preliminary study to understand the mechanism of the uptake of the probes. As shown in Figure 2b, we first incubate HeLa cells with **1a** at 4 and 37 °C, respectively. The fluorescence in cell milieu reduces significantly at 4 °C, suggesting that the uptake is an energy-dependent process. Then we use inhibitors of different endocytotic processes to determine the possible pathways of cellular uptake. We use methyl-β-cyclodextrin (Mβ-CD) for inhibiting lipid raft-dependent endocytosis, chlorpromazine (CPZ) for clathrin-mediated endocytosis, ethylisopropylamiloride (EIPA) for macropinocytosis, and filipin III for caveolae-mediated endocytosis. We find that only the addition of Mβ-CD results in significance decrease of fluorescence, suggesting that the probes likely mainly enter the cells via lipid raft-dependent endocytosis. We also carry out the same experiments using Saos-2 cells and find that the addition of Mβ-CD results in moderate decrease of fluorescence (Figure 2c). These results indicate that the lipid raft-dependent endocytosis of HeLa cells

differs from that of Saos-2, though the exact origin of such a difference remains to be elucidated.

In conclusion, the D-peptide conjugated molecular probes containing a quinazolinone derivative are suitable for selectively imaging intracellular phosphatases of live cells. Moreover, our results confirm the designed molecular probes not only preserving the sensitivity and excellent imaging contrast of commercially available ELF®97, also eliminating the uncontrolled formation of microcrystals without compromising the non-diffusiveness of the probes. Because the molecular probes are suitable for activity profiling of phosphatases in live cells (i.e., it omits cell fixation), and yield reproducible results, they will provide a facile means to target intracellular phosphatases for understanding the characteristics of the intracellular phosphatases, especially their activities. It should provide useful insights for developing applications based on enzymatic reactions, such as instructed-assemblies[11c, 25, 27-28] for molecular imaging and cancer therapy, screening intracellular phosphatases inhibitors using cell assays, and understanding of the biochemical underpinnings of intracellular phosphatases (e.g., PTPs) regulation in both health and disease tissues. Future work will extend to use other sequences conjugated probes to increase the specificity of intracellular phosphatase probes.

Supplementary Material

Refer to Web version on PubMed Central for supplementary material.

Acknowledgements

This work was partially supported by NIH (R01CA142746, R21 AI130560). JZ is an HHMI international student fellow.

References

[1]. Lodish H, Berk A, Kaiser CA, Krieger M, Bretscher A, Ploegh H, Amon A, Scott MP, Mol. Cell Biol. 7th ed., W. H. Freeman, 2012.

[2]. a)Khalil AM, Cambier JC, Shlomchik MJ, Science 2012, 336, 1178–1181; [PubMed: 22555432] b)Vivier E, Nunes JA, Vely F, Science 2004, 306, 1517–1519. [PubMed: 15567854]

[3]. Broberg CA, Zhang LL, Gonzalez H, Laskowski-Arce MA, Orth K, Science 2010, 329, 1660–1662. [PubMed: 20724587]

[4]. a)Fishman WH, Inglis NR, Green S, Anstiss CL, Gosh NK, Reif AE, Rustigia R, Krant MJ, Stolbach LL, Nature 1968, 219, 697–699; [PubMed: 5691166] b)Pospisil P, Iyer LK, Adelstein SJ, Kassis AI, BMC Bioinform. 2006, 7, 354–364;c)Ruark E, Snape K, Humburg P, Loveday C, Bajrami I, Brough R, Rodrigues DN, Renwick A, Seal S, Ramsay E, Duarte SD, Rivas MA, Warren-Perry M, Zachariou A, Campion-Flora A, Hanks S, Murray A, Pour NA, Douglas J, Gregory L, Rimmer A, Walker NM, Yang TP, Adlard JW, Barwell J, Berg J, Brady AF, Brewer C, Brice G, Chapman C, Cook J, Davidson R, Donaldson A, Douglas F, Eccles D, Evans DG, Greenhalgh L, Henderson A, Izatt L, Kumar A, Lalloo F, Miedzybrodzka Z, Morrison PJ, Paterson J, Porteous M, Rogers MT, Shanley S, Walker L, Gore M, Houlston R, Brown MA, Caufield MJ, Deloukas P, McCarthy MI, Todd JA, Turnbull C, Reis JS, Ashworth A, Antoniou AC, Lord CJ, Donnelly P, Rahman N, Nature 2013, 493, 406–410; [PubMed: 23242139] d)Saha S, Bardelli A, Buckhaults P, Velculescu VE, Rago C, St Croix B, Romans KE, Choti MA, Lengauer C, Kinzler KW, Vogelstein B, Science 2001, 294, 1343–1346. [PubMed: 11598267]

[5]. Bates JM, Akerlund J, Mittge E, Guillemin K, Cell Host & Microbe 2007, 2, 371–382. [PubMed: 18078689]

[6]. Zuk PA, Zhu M, Ashjian P, De Ugarte DA, Huang JI, Mizuno H, Alfonso ZC, Fraser JK, Benhaim P, Hedrick MH, Mol. Biol. Cell 2002, 13, 4279–4295. [PubMed: 12475952]

[7]. Katagiri T, Yamaguchi A, Komaki M, Abe E, Takahashi N, Ikeda T, Rosen V, Wozney JM, Fujisawasehara A, Suda T, J. Cell Biol. 1994, 127, 1755–1766. [PubMed: 7798324]

[8]. Fonta C, Négyessy L, Subcell. Biochem. 2015, 76, 85–106. [PubMed: 26219708]

[9]. a)Uhlén M, Pontén F, Lindskog C, Science 2015, 347, 1274–1274;b)Millán JL, Mammalian alkaline phosphatases: from biology to applications in medicine and biotechnology, John Wiley & Sons, 2006.

[10]. Liberti S, Sacco F, Calderone A, Perfetto L, Iannuccelli M, Panni S, Santonico E, Palma A, Nardozza AP, Castagnoli L, Cesareni G, Febs J 2013, 280, 379–387. [PubMed: 22804825]

[11]. a)Ye FM, Wu CF, Jin YH, Chan YH, Zhang XJ, Chiu DT, J. Am. Chem. Soc. 2011, 133, 8146–8149; [PubMed: 21548583] b)Mutch SA, Gadd JC, Fujimoto BS, Kensel-Hammes P, Schiro PG, Bajjalieh SM, Chiu DT, Nat. Protoc. 2011, 6, 1953–1968; [PubMed: 22094731] c)Ye DJ, Shuhendler AJ, Cui LN, Tong L, Tee SS, Tikhomirov G, Felsher DW, Rao JH, Nat. Chem. 2014, 6, 519–526; [PubMed: 24848238] d)Liang G, Ren H, Rao J, Nat Chem 2010, 2, 54–60; [PubMed: 21124381] e)Shuhendler AJ, Pu KY, Cui L, Uetrecht JP, Rao JH, Nat. Biotechnol. 2014, 32, 373–380. [PubMed: 24658645]

[12]. Sacco F, Perfetto L, Castagnoli L, Cesareni G, FEBS Lett. 2012, 586, 2732–2739. [PubMed: 22626554]

[13]. Lorenz U, Curr. Protoc. Immunol. 2011, Chapter 11, Unit 11.17.

[14]. Larison KD, Bremiller R, Wells KS, Clements I, Haugland RP, J. Histochem. Cytochem. 1995, 43, 77–83. [PubMed: 7822768]

[15]. Cox WG, Singer VL, J. Histochem. Cytochem. 1999, 47, 1443–1455. [PubMed: 10544217]

[16]. Wang KT, Kirichian AM, Al Aowad AF, Adelstein SJ, Kassis AI, Bioconjug. Chem. 2007, 18, 754–764. [PubMed: 17385903]

[17]. Kim TI, Kim H, Choi Y, Kim Y, Chem. Commun. 2011, 47, 9825–9827.

[18]. a)Wang H, Feng Z, Del Signore SJ, Rodal AA, Xu B, J. Am. Chem. Soc. 2018, 140, 3505–3509; [PubMed: 29481071] b)Zhou J, Du X, Berciu C, He H, Shi J, Nicastro D, Xu B, Chem 2016, 1, 246–263. [PubMed: 28393126]

[19]. Yu Z-H, Zhang Z-Y, Chem. Rev. 2018, 118, 1069–1091. [PubMed: 28541680]

[20]. Feng Z, Wang H, Du X, Shi J, Li J, Xu B, Chem. Comm. 2016, 52, 6332–6335. [PubMed: 27087169]

[21]. Du X, Zhou J, Shi J, Xu B, Chem. Rev. 2015, 115, 13165–13307. [PubMed: 26646318]

[22]. Weng C, Peter D, Fmoc Slild Phase Peptide Synthesis: A Practical Approach, Oxford: Oxford University Press, 2000.

[23]. Pires RA, Abul-Haija YM, Costa DS, Novoa-Carballal R, Reis RL, Ulijn RV, Pashkuleva I, J. Am. Chem. Soc. 2015, 137, 576–579. [PubMed: 25539667]

[24]. Dahl R, Sergienko EA, Su Y, Mostofi YS, Yang L, Simao AM, Narisawa S, Brown B, Mangravita-Novo A, Vicchiarelli M, Smith LH, O'Neill WC, Millan JL, Cosford NDP, J. Med. Chem. 2009, 52, 6919–6925. [PubMed: 19821572]

[25]. Gao Y, Shi J, Yuan D, Xu B, Nat. Comm. 2012, 3, 1033–1040.

[26]. a)Hunter T, Cold Spring Harbor Perspect. Biol 2014, 6, a020644;b)Sawyers C, Nature 2004, 432, 294–297. [PubMed: 15549090]

[27]. Li J, Bullara D, Du X, He H, Sofou S, Kevrekidis IG, Epstein IR, Xu B, ACS nano 2018, 12, 3804–3815. [PubMed: 29537820]

[28]. a)Zhou J, Du X, Li J, Yamagata N, Xu B, J. Am. Chem. Soc. 2015, 137, 10040–10043; [PubMed: 26235707] b)Feng Z, Wang H, Chen X, Xu B, J. Am. Chem. Soc. 2017, 139, 15377–15384; [PubMed: 28990765] c)Kuang Y, Xu B, Angew. Chem. Int. Ed. 2013, 52, 6944–6948;d)Zhan J, Cai Y, He S, Wang L, Yang Z, Angew. Chem. Int. Ed. 2018, 57, 1813–1816;e)Hai Z, Li J, Wu J, Xu J, Liang G, J. Am. Chem. Soc. 2017, 139, 1041–1044; [PubMed: 28064496] f)Kumar M, Ing NL, Narang V, Wijerathne NK, Hochbaum AI, Ulijn RV, Nat. Chem. 2018, 10, 696–703; [PubMed: 29713031] g)Yu G, Zhang M, Saha ML, Mao Z, Chen J, Yao Y, Zhou Z, Liu Y, Gao C, Huang F, Chen X, Stang PJ, J. Am. Chem. Soc. 2017, 139, 15940–15949; [PubMed: 29019660]

h)Aggarwal BB, Harikumar KB, Int. J. Biochem. Cell Biol. 2009, 41, 40–59; [PubMed: 18662800] i)Li J, Xie C, Huang J, Jiang Y, Miao Q, Pu K, Angew. Chem. Int. Ed. 2018, 57, 3995–3998.

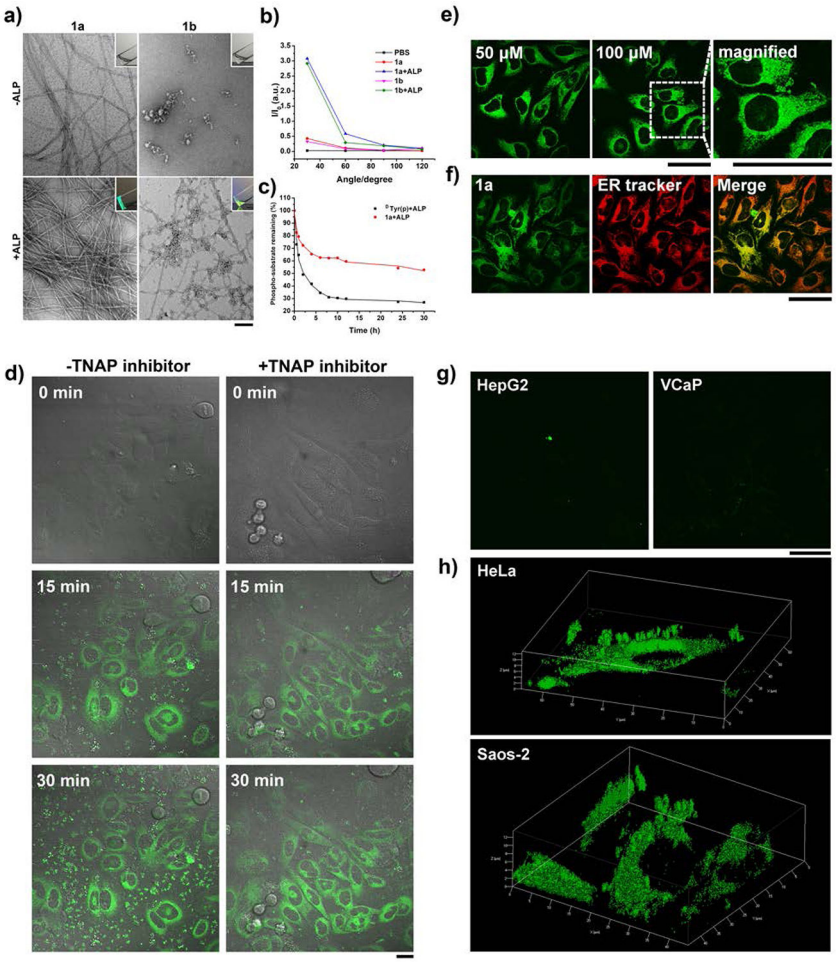

Figure 1.

(a) TEM images of the solutions of **1a** and **1b** (0.5 wt%) without or with the addition of ALP at physiological pH (pH = 7.4) in PBS buffer (insert: corresponding optical images; [ALP] = 1 U/mL; bar = 100 nm). (b) Static light scattering (SLS) signals of the solutions of **1a** and **1b** before and after the treatment of ALP at the concentration of 100 μM ([ALP] = 1 U/mL). (c) Time-dependent dephosphorylation process of the precursor **1a** with the addition of ALP at 37 °C in PBS buffer ($[\mathbf{1a}]_0$ = 200 μM, [ALP] = 0.1 U/mL). (d) Fluorescent confocal microscopy images show the fluorescence emission in Saos-2 cells with the treatment of **1a** at the concentration of 250 μM for 0 min, 15 min and 30 min, respectively. [TNAP inhibitor] = 5 μM; scale bar = 20 μm. (e) Fluorescent confocal microscopy images show the fluorescence emission in HeLa cells with the treatment of **1a** at different concentrations (50 μM and 100 μM) for 4 h, respectively. (f) Fluorescent confocal microscopy images of HeLa cells treated with **1a** at the concentration of 50 μM for 4 h and then stained with endoplasmic reticulum (ER) tracker. Pearson's *R* value is 0.725 from 30 cells. Scale bar = 50 μm. (g) Fluorescent confocal microscopy images show the fluorescence in different cell lines (HepG2 and VCaP) with the treatment of **1a** at the concentration of 50 μM for 4 h, respectively. Scale bar = 50 μm. (h) 3D construction of HeLa and Saos-2 cells with the treatment of **1a** at the concentration of 50 μM for 4 h, respectively.

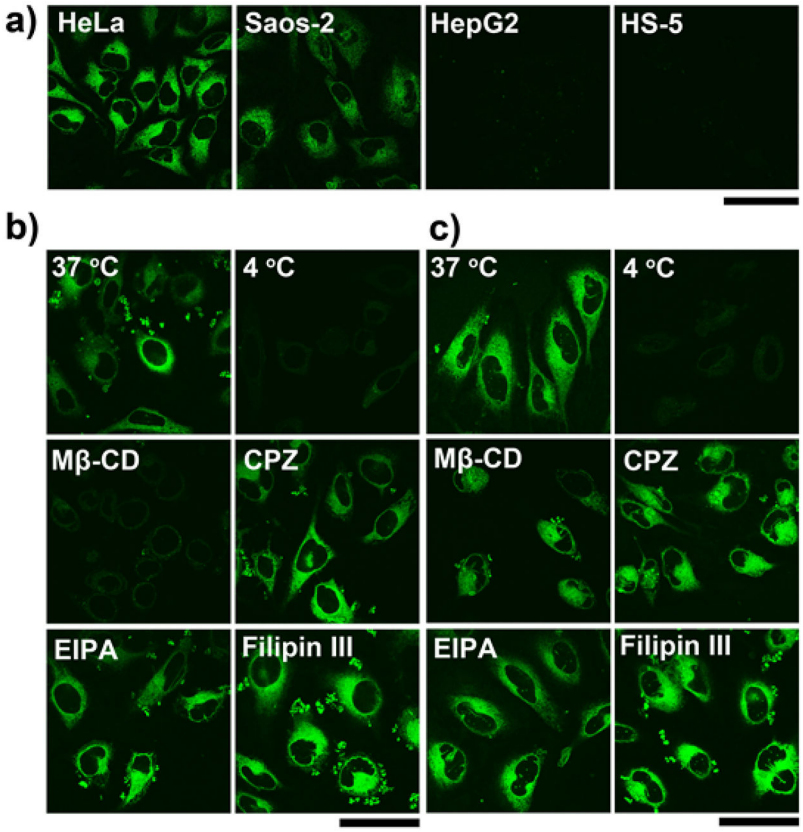

Figure 2.

(a) Fluorescent confocal microscopy images show the fluorescence emission in different cell lines (HeLa, Saos-2, HepG2 and HS-5) with the treatment of **1b** at the concentration of 50 μM for 4 h, respectively. Scale bar = 50 μm. Fluorescent confocal microscopy images show the fluorescence emission in (b) HeLa and (c) Saos-2 cells with the treatment of **1a** at 37 °C and 4 °C, or with the treatment of **1a** plus Mβ-CD, CPZ, EIPA and filipin III at 37 °C for 4 h, respectively. [**1a**] = 50 μM, [Mβ-CD] = 5 mM, [CPZ] = 30 μM, [EIPA] = 50 μM, [filipin III] = 5 μg/mL. Scale bar = 50 μm.

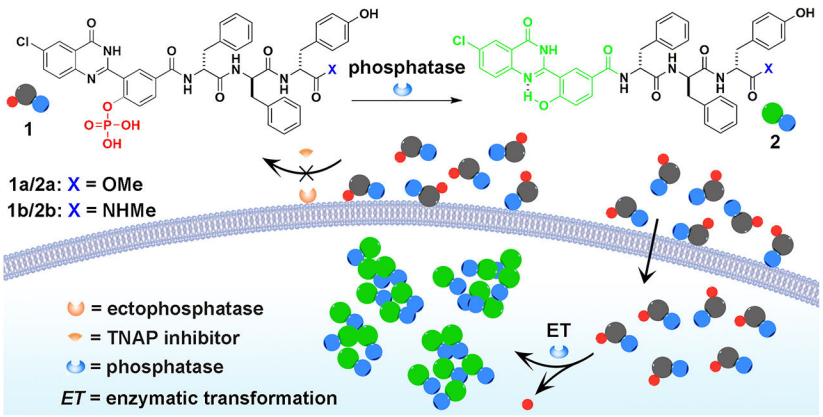

Scheme 1.

Schematic illustration of conjugating a D-tripeptide to the motif of a phosphatase probe (i.e., a quinazolinone derivative) that generates a cell-compatible, biostable, and non-diffusive functional probe for selectively imaging intracellular phosphatases.